AGU PUBLICATIONS

JGR

Journal of Geophysical Research: Space Physics

RESEARCH ARTICLE

10.1002/2017JA023972

Key Points:
- A soliton model for generation of electrostatic waves observed in the lunar wake during the first flyby of the ARTEMIS mission is proposed
- Slow and fast ion-acoustic solitons and electron-acoustic solitons can exist in the lunar wake
- Predicted amplitudes and frequency range of the electrostatic waves are in excellent agreement with lunar wake observations

Correspondence to:
S. V. Singh,
satyavir@iigs.iigm.res.in

Citation:
Rubia, R., S. V. Singh, and G. S. Lakhina (2017), Occurrence of electrostatic solitary waves in the lunar wake, *J. Geophys. Res. Space Physics*, *122*, 9134–9147, doi:10.1002/2017JA023972.

Received 4 FEB 2017
Accepted 8 JUL 2017
Accepted article online 13 JUL 2017
Published online 24 SEP 2017

Occurrence of electrostatic solitary waves in the lunar wake

R. Rubia[1], S. V. Singh[1], and G. S. Lakhina[1]

[1]Indian Institute of Geomagnetism, Navi Mumbai, India

Abstract An alternative generation mechanism for the electrostatic waves observed in the lunar wake during the first flyby of the Acceleration, Reconnection, Turbulence and Electrodynamics of the Moon's Interaction with the Sun (ARTEMIS) mission in terms of slow and fast ion-acoustic and electron-acoustic solitons is proposed. The lunar wake plasma is modeled by fluid multicomponent magnetized plasma comprising hot protons, hot heavier ions, α particles (He^{++}), electron beam, and suprathermal electrons following kappa distribution. The electric fields associated with the slow and fast ion-acoustic and electron-acoustic solitons are in the range of ∼(0.0003–17) mV m^{-1}. This is in excellent agreement with observed electrostatic wave electric field of 5 to 15 mV m^{-1}. The fast Fourier transform of soliton electric fields generates broadband spectra having peak frequencies (corresponding to peak in the power spectra) in the range of ∼(3–1800) Hz. This corresponds to wave frequencies being in the range of ∼(0.001–0.56)f_{pe}, where f_{pe} is the electron plasma frequency. This matches well with the observed frequency range of (0.01–0.4) f_{pe}. Further, the widths and velocities of these solitons are in the range ∼(100–8000) m and ∼(30–1300) km s^{-1}, respectively. Both, soliton widths and velocities, match well with the estimated wavelengths (a few hundred meters to a couple of thousand meters) and estimated phase velocities (of the order of 1000 km s^{-1}) of the electrostatic waves in the lunar wake.

1. Introduction

Electrostatic solitary waves (ESWs) are ubiquitous in space plasmas. They have been observed in various regions of Earth's magnetosphere, e.g., cusp region [*Pickett et al.*, 2001], auroral region [*Ergun et al.*, 1998], plasma sheet boundary layer (PSBL) [*Matsumoto et al.*, 1994], magnetotail [*Kojima et al.*, 1997], magnetopause [*Matsumoto et al.*, 2003], magnetosheath [*Pickett et al.*, 2003], and bow shock [*Bale et al.*, 1998], and in the solar wind plasma at about 1 AU [*Mangeney et al.*, 1999]. The observations by SELENE (KAGUYA) spacecraft substantiate the existence of ESWs in the solar wind and in the lunar wake [*Hashimoto et al.*, 2010].

Since the advent of the space age, the interaction of moon with the solar wind has been continuously investigated. On the basis of the observations of Lunar Explorer 35 which was injected in the selenocentric orbit to investigate the magnetic field of the moon and the interaction of the solar wind with the lunar body, *Ness et al.* [1967] gave conclusive evidence of the existence of lunar wake and the absence of intrinsic lunar magnetic field.

When the solar wind interacts with the Moon, the solar wind plasmas are absorbed by the lunar surface carving out a lunar wake in the "nightside" of the moon. Due to the absence of intrinsic magnetic field and sufficiently low conductivity of the Moon, the solar wind magnetic field easily penetrates the Moon as compared to the solar wind particles. The density gradients drive the solar wind plasma to refill the wake region by ambipolar diffusion [*Ogilvie et al.*, 1996; *Wiehle et al.*, 2011; *Tao et al.*, 2012].

The Wind spacecraft, launched in 1994, made many close approaches to the moon at roughly 6.5R_L for gravity-assisted orbit changes. Here R_L is the lunar radius, R_L = 1738 km. *Ogilvie et al.* [1996] analyzed the observations made by Wind and reported that the plasma density decreased exponentially from the periphery of the wake toward the center. They found that the electron temperature increases in the wake while the ion temperature remains fairly constant. *Bosqued et al.* [1996] reported a gradual decrease of electron and ion densities to a value <0.5 cm^{-3} near the center of the lunar wake.

Tao et al. [2012] presented a detailed analysis of the electrostatic waves, in the frequency range ∼10 Hz to ∼6 kHz with parallel electric field amplitudes of ∼5 to 15 mV m^{-1}, observed by the Acceleration, Reconnection, Turbulence and Electrodynamics of the Moon's Interaction with the Sun (ARTEMIS) mission on the outbound

side of the flyby. The Time History of Events and Macroscale Interactions during Substorms (THEMIS) mission constitutes an array of five spacecrafts. The ARTEMIS mission is a new two-probe lunar mission derived from THEMIS, which uses the two outermost spacecrafts of the THEMIS constellation. It utilizes THEMIS-B and THEMIS-C which are designated as P1 and P2, respectively. ARTEMIS P1 made the first lunar wake flyby of the mission on 13 February 2010. The first flyby occurred at $3.5R_L$ downstream from the moon. The ARTEMIS mission covers an extensive range of lunar wake (1.1 – 12) R_L [*Wiehle et al.*, 2011; *Tao et al.*, 2012].

Tao et al. [2012] performed 1-D Vlasov simulation on a four-component lunar wake plasma comprising protons, ions, electron beam, and suprathermal electrons to identify the wave modes. They considered both the suprathermal electrons and the beam electrons to follow κ distribution. They concluded that the observed electrostatic waves, in the frequency range (0.1 – 0.4) f_{pe}, were most likely the electron beam mode. Further, they discussed that although they did not observe well-defined ESWs, the possibility of the occurrence of the ESWs in the lunar wake was not completely ruled out. In fact, *Hashimoto et al.* [2010] have observed ESWs in the lunar wake. David Malaspina (private communication, 2017) has frequently observed ESWs in the lunar wake on many ARTEMIS flybys of lunar wake. A reason for not observing solitary waves in simulations could be that *Tao et al.* [2012] did not run the simulation for a long enough time [*Miyake et al.*, 2000; *Umeda et al.*, 2004].

Over the past several decades, the observation of the ESWs in the Earth's magnetosphere has motivated the extensive study of ESWs in both unmagnetized and magnetized multispecies plasma [*Sagdeev*, 1966; *Washimi and Taniuti*, 1966; *Buti*, 1980; *Kakad et al.*, 2007; *Lakhina et al.*, 2008a, 2008b, 2009; *Devanandhan et al.*, 2012; *Rufai et al.*, 2012; *Singh et al.*, 2013; *Olivier et al.*, 2015; *Kakad et al.*, 2016]. *Lakhina et al.* [2008b] investigated the unmagnetized four-component plasma comprising hot ions, hot ion beam, cold electrons, and electron beam. They found that three modes, viz., slow and fast ion-acoustic mode and electron-acoustic mode, exist. The slow ion-acoustic mode was found to have the least critical Mach number. *Lakhina et al.* [2011] proposed a generation mechanism for the broadband electrostatic waves observed in the PSBL region by Cluster spacecraft in terms of electron-acoustic solitons and double layers. It was shown that these short electric field pulses, when Fourier transformed to the frequency domain, could produce the observed broadband electrostatic noise in the frequency range of ~220 Hz to 10 kHz. Ion-acoustic solitons were analyzed in a three-component plasma comprising cold heavier ions, warm lighter ions, and Boltzmann-distributed hot electrons by *Lakhina et al.* [2014]. When the thermal effects of the lighter ion species are taken into account, in addition to the usual fast ion-acoustic mode, a slow ion-acoustic mode appears. It was found that the fast ion-acoustic mode supports only positive potential solitons, while slow ion-acoustic mode supports both positive and negative potential solitons and double layers. *Lakhina and Singh* [2015] extended their model and considered hot heavier ions streaming with finite velocity with respect to the lighter ions and electrons having κ distribution. They provided a generation mechanism for weak double layers and low-frequency coherent electrostatic waves observed in the solar wind at 1 AU by Wind spacecraft in terms of slow and fast ion-acoustic solitons and double layers. *Rubia et al.* [2016] analyzed a three-component plasma model comprising hot protons, hot heavier ions (He^{++}), and suprathermal electrons with κ distribution. They applied the model to explain the coherent electrostatic structures observed in the solar wind at 1 AU.

In this paper, we propose an alternate model for the electrostatic waves reported by *Tao et al.* [2012] in lunar wake in terms of ion- and electron-acoustic solitons. We use a four-component fluid plasma model comprising protons, heavier ions (He^{++}), electron beam, and suprathermal electrons following κ distribution. We are able to explain the characteristics of observed low- and high-frequency waves in the lunar wake in terms of fast Fourier transform (FFT) of the ESWs. We emphasize that our model deals with the time-stationary state of the plasma system when the plasma instabilities, if excited initially by the electron beam, have saturated. The model deals with the nonlinear modes of the system.

The paper is organized as follows. Section 2 summarizes the observations and the outcomes of the 1-D Vlasov simulations of the electrostatic waves observed in the lunar wake by *Tao et al.* [2012]. In section 3, an overview of the theoretical model considered for the lunar wake is provided. Section 4 describes the numerical results pertaining to the theoretical model. Section 5 discusses the application of the model to electrostatic waves observed in lunar wake. Section 6 gives the conclusions.

2. Observations

Figure 1 illustrates an overview of the observations of lunar wake flyby (figure reproduced from *Tao et al.* [2012]). The two vertical black dashed lines in the figure show the interval in which the ARTEMIS P1 crossed the

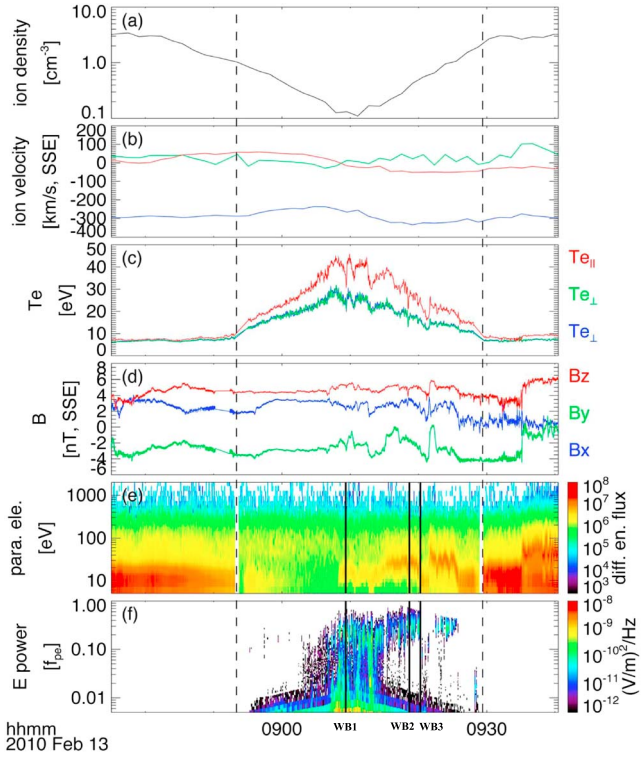

Figure 1. The figure depicts the overview observations of the first lunar wake flyby of the ARTEMIS mission. The two vertical dashed lines correspond to the duration in which the flyby crossed the lunar shadow. (a) Ion density. (b) Ion velocity in selenocentric solar ecliptic (SSE) coordinates. (c) Electron temperature; here the red line corresponds to the field-aligned temperature ($T_{e\|}$), and the green and blue lines correspond to the perpendicular temperatures ($T_{e\perp}$). The green line fully overlaps the blue line as there is no special preference in perpendicular temperatures. (d) Magnetic field in SSE coordinates. (e) Differential energy flux of parallel electrons. (f) Electric field power spectrum from the onboard digital field board. Here frequency is normalized by the local electron plasma frequency (f_{pe}). The three vertical bars in Figures 1e and 1f indicate the times of three wave bursts which are analyzed in detail in the paper. These wave bursts are designated as WB1, WB2, and WB3 according to their temporal order of occurrence. Reprinted from *Tao et al.* [2012]—Kinetic instabilities in the lunar wake: ARTEMIS observations, *J. Geophys. Res.*, 117, A03106.

lunar shadow. Figure 1a indicates that the density decreases exponentially toward the center of the wake. The flow velocity is found to be relatively stable during the flyby (Figure 1b). The electron temperature T_e variation is found to be nearly isotropic outside the wake (Figure 1c). While inside the wake both the field-aligned temperature and perpendicular temperature increase, with the former increasing more. The observed magnetic field and the differential energy flux of the parallel electrons are depicted in Figures 1d and 1e, respectively.

Figure 1f shows the electric field power spectrum. The frequency range of the waves lies mostly between $0.1f_{pe}$ and $0.4f_{pe}$. However, in the middle of the flyby the power occasionally reduces to $0.01f_{pe}$; f_{pe} is the electron plasma frequency. These waves were interpreted as electrostatic waves as no corresponding magnetic field signals were observed. The black vertical lines across Figures 1e and 1f specify the times of the three high time resolution wave bursts. The three wave bursts are labeled as WB1, WB2, and WB3 in a temporal order of their occurrence as shown in the figure.

Tao et al. [2012] reported the local values of Debye length, λ_d roughly as 108 m, 53 m, and 46 m for WB1, WB2, and WB3, respectively. Moreover, they reported that the low-frequency waves with frequency $0.01f_{pe}$ were observed at the time of WB1. They did not provide a detailed analysis for the observed low-frequency waves at WB1; however, they proposed the ion dynamics to be involved in the generation of the low-frequency waves. From their Figure 3 (refer to *Tao et al.* [2012]) the parallel electric field amplitude of the electrostatic waves for WB1 varies from ~3 to 18 mV m^{-1} (Panel (a)), while the amplitude varies as ~1 to 7 mV m^{-1} for WB2 (Panel (c)) and from ~5 to 15 mV m^{-1} (Panel (e)) for WB3. The parameters corresponding to WB2 and WB3 were found to be similar. Hence, in this paper their combined analysis will be referred to as WB2/WB3. From simulation, they reported that the electric field amplitude for WB2/WB3 is roughly 2 mV m^{-1}, which is considerably smaller

Table 1. The Parameters Corresponding to the High Time Resolution Wave Bursts at the Time of WB1 and WB2/WB3 [*Tao et al.*, 2012]

	WB1	WB2/WB3
λ_d (m)	108	50
n_0 (cm^{-3})	0.13	0.5
T_e (eV)	28	22.64
f_{pe} (Hz)	3237.785	6349.82

than the observed wave amplitudes. Table 1 enlists the parameters corresponding to WB1 and WB2/WB3 that are utilized for analysis in this paper and are taken from Figure 1. Further, from the cross-correlation analysis they found the phase velocity of the wave corresponding to WB1 as 2151 km s^{-1}, while for WB2 the phase velocity is 1568 km s^{-1} and 1397 km s^{-1} for WB3. From the cross-spectrum analysis they found the wavelength corresponding to WB1 as 1727 m. The wavelength for WB2 was found to be 272 m and for WB3 as 231 m.

3. Ion- and Electron-Acoustic Soliton Model

We model the lunar wake plasma by a homogeneous, collisionless, and magnetized four-component plasma comprising protons (N_{p0} and T_p), heavier ions, i.e, alpha particles, He^{++} (N_{i0} and T_i), electron beam (N_{b0}, T_b, and V_{b0}), and suprathermal electrons (N_{e0} and T_e). Here N_{j0} and T_j represent the equilibrium values of the density and temperature of the species j, and $j = p, i, b$, and e for protons, heavier ions, electron beam, and suprathermal electrons, respectively. V_{b0} is the drift velocity of the beam electron (along the direction of the ambient magnetic field, $\vec{B}_0$).

We consider the suprathermal electrons in the lunar wake to follow the κ (Kappa) distribution given by [*Summers and Thorne*, 1991]

$$f_e(v) = \frac{N_{e0}}{\sqrt{\pi}\theta} \frac{\Gamma(\kappa)}{\sqrt{\kappa}\Gamma(\kappa - 1/2)} \left(1 + \frac{v^2}{\kappa\theta^2}\right)^{-\kappa} \tag{1}$$

Here $\Gamma(\kappa)$ is the gamma function. κ is the spectral index with $\kappa > 3/2$, and θ is the modified electron thermal speed given by

$$\theta^2 = \left(2 - \frac{3}{\kappa}\right) \frac{T_e}{m_e}$$

Here T_e and m_e are the temperature and mass of electron, respectively. When $\kappa \to \infty$, the κ distribution approaches a Maxwellian distribution, i.e, attains thermal equilibrium [*Lakhina and Singh*, 2015].

The number density of the suprathermal electrons in the presence of electrostatic wave having electric potential, ϕ, can be obtained by replacing $\frac{v^2}{\theta^2}$ by $\frac{v^2}{\theta^2} - \frac{2e\phi}{m\theta^2}$ in equation (1) and integrating it over the velocity space [*Devanandhan et al.*, 2011]

$$n_e = n_{e0} \left(1 - \frac{\phi}{\kappa - 3/2}\right)^{-\kappa+1/2} \tag{2}$$

The nonlinear electrostatic waves are considered to be propagating parallel to the ambient magnetic field. The dynamics of protons, heavier ions, and electron beam in the lunar wake plasma is governed by the following normalized multifluid equations:

the continuity equation

$$\frac{\partial n_j}{\partial t} + \frac{\partial (n_j v_j)}{\partial x} = 0 \tag{3}$$

the momentum equation

$$\frac{\partial v_j}{\partial t} + v_j \frac{\partial v_j}{\partial x} + Z_j \mu_{pj} \frac{\partial \phi}{\partial x} + 3\mu_{pj}\sigma_j \frac{n_j}{n_{j0}^2} \frac{\partial n_j}{\partial x} = 0 \tag{4}$$

and Poisson's equation

$$\frac{\partial^2 \phi}{\partial x^2} = (n_e + n_b - n_p - Z_i n_i) \tag{5}$$

Equation (4) combines both the momentum equation and equation of state.

In equations (2)–(5), the number densities are normalized by total equilibrium number density, $N_0 = N_{p0} + Z_i N_{i0} = N_{e0} + N_{b0}$; velocities are normalized with the ion-acoustic speed defined by electron temperature and

proton mass $C_a = \sqrt{T_e/m_p}$, lengths with the effective hot electron Debye length $\lambda_{de} = \sqrt{T_e/4\pi N_0 e^2}$, time with the inverse of the effective proton plasma frequency $f_{pp} = \sqrt{4\pi N_0 e^2/m_p}$ and electrostatic potential, ϕ by T_e/e. Here $\mu_{pj} = m_p/m_j$, where m_p is the mass of the proton and m_j is the mass of the jth species. $\sigma_j = T_j/T_e$ and $n_{j0} = N_{j0}/N_0$ are the normalized equilibrium number density of jth species. e is the electronic charge. v_j is the normalized fluid velocity. $Z_j = +1$ for protons, $Z_j = +2$ for heavier ions (alpha particles), and $Z_j = -1$ for beam electrons. We have considered the adiabatic index $\gamma_j = 3$ for all species. This is justified for a one-dimensional case considered here.

To analyze the properties of arbitrary amplitude electrostatic solitary waves, we transform the above set of equations to a stationary frame moving with velocity V, the phase velocity of the electrostatic solitary wave, i.e., $\xi = x - Mt$, where $M = V/C_a$ represents the Mach number with respect to the ion-acoustic speed. Further, solving for the perturbed number densities of protons, heavier ions, and electron beam, substituting these expressions in the Poisson equation, and assuming appropriate boundary conditions for the localized disturbances along with the conditions that electrostatic potential $\phi = 0$, and $d\phi/d\xi = 0$ at $\xi \to \pm\infty$, we obtain the energy integral as

$$\frac{1}{2}\left(\frac{d\phi}{d\xi}\right)^2 + S(\phi, M) = 0 \tag{6}$$

Equation (6) describes the motion of pseudoparticle of unit mass in a pseudopotential $S(\phi, M)$, where ϕ and ξ play the role of displacement from the equilibrium and time, respectively [*Lakhina et al.*, 2009]. Here the Sagdeev pseudopotential, $S(\phi, M)$, is given by

$$\begin{aligned} S(\phi, M) = {} & \frac{n_{p0}}{6\sqrt{3\sigma_p}}\left\{\left(M + \sqrt{3\sigma_p}\right)^3 - \left[\left(M + \sqrt{3\sigma_P}\right)^2 - 2\phi\right]^{3/2}\right. \\ & \left. -\left(M - \sqrt{3\sigma_p}\right)^3 + \left[\left(M - \sqrt{3\sigma_p}\right)^2 - 2\phi\right]^{3/2}\right\} \\ & + \frac{n_{i0}}{6\sqrt{3\sigma_i}}\left\{\left(\frac{M}{\sqrt{\mu_{pi}}} + \sqrt{3\sigma_i}\right)^3 - \left[\left(\frac{M}{\sqrt{\mu_{pi}}} + \sqrt{3\sigma_i}\right)^2 - 2Z_i\phi\right]^{3/2}\right. \\ & \left. -\left(\frac{M}{\sqrt{\mu_{pi}}} - \sqrt{3\sigma_i}\right)^3 + \left[\left(\frac{M}{\sqrt{\mu_{pi}}} - \sqrt{3\sigma_i}\right)^2 - 2Z_i\phi\right]^{3/2}\right\} \\ & + \frac{n_{b0}}{6\sqrt{3\sigma_b}}\left\{\left(\frac{M - V_{b0}}{\sqrt{\mu_{\mathrm{pe}}}} + \sqrt{3\sigma_b}\right)^3 - \left[\left(\frac{M - V_{b0}}{\sqrt{\mu_{\mathrm{pe}}}} + \sqrt{3\sigma_b}\right)^2 + 2\phi\right]^{3/2}\right. \\ & \left. + \left[\left(\frac{M - V_{b0}}{\sqrt{\mu_{\mathrm{pe}}}} - \sqrt{3\sigma_b}\right)^2 + 2\phi\right]^{3/2} - \left(\frac{M - V_{b0}}{\sqrt{\mu_{\mathrm{pe}}}} - \sqrt{3\sigma_b}\right)^3\right\} \\ & + n_{e0}\left[1 - \left(1 - \frac{\phi}{\kappa - 3/2}\right)^{-\kappa + 3/2}\right] \end{aligned} \tag{7}$$

Equation (7) has been written in symbolic form where the operation of a square root on a squared expression returns the same expression, e.g., $\sqrt{(M \pm \sigma_j)^2} = M \pm \sigma_j$.

Equation (6) gives a soliton solution when the pseudoparticle is reflected in the pseudopotential field and returns to its initial state; i.e., the pseudoparticle experiences a zero potential drop [*Lakhina et al.*, 2011]. Therefore, for the existence of soliton solutions, the Sagdeev pseudopotential $S(\phi, M)$ must satisfy the following conditions: (i) $S(\phi, M) = 0$, $dS(\phi, M)/d\phi = 0$, and $d^2S(\phi, M)/d\phi^2 < 0$ at $\phi = 0$, (ii) $S(\phi, M) = 0$ at $\phi = \phi_{\max}$ ($\phi_{\max}$ is the maximum attainable amplitude of the soliton), and (iii) $S(\phi, M) < 0$ for $0 < |\phi| < |\phi_{\max}|$. When these conditions are satisfied, we obtain solitary wave solution.

From equation (7), it can be seen that the Sagdeev pseudopotential, $S(\phi, M)$, and its first derivative with respect to ϕ vanish at $\phi = 0$. Further, the soliton condition $\mathrm{d}^2S(\phi, M)/\mathrm{d}\phi^2 < 0$ at $\phi = 0$ is satisfied provided $M > M_0$, where the critical Mach number, M_0, satisfies the following equation:

$$\frac{n_{p0}}{M^2 - 3\sigma_p} + \frac{n_{i0}Z_i^2}{\frac{M^2}{\mu_{pi}} - 3\sigma_i} + \frac{n_{b0}}{\frac{(M - V_{b0})^2}{\mu_{\mathrm{pe}}} - 3\sigma_b} = n_{e0}\left(\frac{2\kappa - 1}{2\kappa - 3}\right) \tag{8}$$

Critical Mach number, M_0, represents the minimum permissible Mach number for the solitary solutions to exist. The essential requirement for the generation of the solitary waves is that the Mach number $M > M_0$, given by equation (8). For the parameters relevant to the lunar wake plasma, the critical Mach numbers, M_0, are obtained by numerically solving equation (8). In general, we obtain six roots from equation (8), but all the roots are not physical. Here we consider only real positive roots for M_0. Equation (8) yields three positive roots. The smallest root corresponds to the slow ion-acoustic mode, and the intermediate root corresponds to the fast ion-acoustic mode. The largest root corresponds to the electron-acoustic mode [*Lakhina et al.*, 2008b]. The fast ion-acoustic mode is similar to the ion-acoustic mode of proton-electron plasma. The slow ion-acoustic mode is a new mode that occurs due to the presence of heavier ions. It is actually an ion-ion hybrid mode that requires essentially two ion species having different thermal velocities or a relative streaming between the ions [*Lakhina and Singh*, 2015].

The third derivative of the Sagdeev pseudopotential, $S(\phi, M)$, evaluated at $\phi = 0$ is given by

$$\left(\frac{\mathrm{d}^3S(\phi, M)}{\mathrm{d}\phi^3}\right)_{\phi=0} = \frac{3n_{p0}(M^2 + \sigma_p)}{(M^2 - 3\sigma_p)^3} + \frac{3n_{i0}Z_i^3\left(\frac{M^2}{\mu_{pi}} + \sigma_i\right)}{\left(\frac{M^2}{\mu_{pi}} - 3\sigma_i\right)^3} - \frac{3n_{b0}\left[\frac{(M - V_{b0})^2}{\mu_{\mathrm{pe}}} + \sigma_b\right]}{\left[\frac{(M - V_{bo})^2}{\mu_{\mathrm{pe}}} - 3\sigma_b\right]^3} - n_{e0}\frac{(4\kappa^2 - 1)}{(2\kappa - 3)^2} \tag{9}$$

The positive (negative) values of equation (9) evaluated at $M = M_0$ corresponds to electrostatic solitons having positive (negative) electrostatic potential, ϕ [*Maharaj et al.*, 2012a, 2012b; *Rubia et al.*, 2016]. Generally, the soliton solution is found to exist for $M > M_0$. However, over the parameter range where coexistence of both polarity solitons is feasible, the solitons are found to have finite amplitude at $M = M_0$ [*Baluku et al.*, 2010].

4. Numerical Results and Discussions

For parameters relevant to the lunar wake plasma, equation (7) is numerically solved for the Sagdeev pseudopotential, $S(\phi, M)$ as a function of ϕ for various values of Mach numbers $M \geq M_0$. When finite amplitude solitons exist at $M = M_0$, we have coexistence of both polarity solitons. Based on the observations provided by *Tao et al.* [2012], we have analyzed our theoretical model of lunar wake plasma. *Tao et al.* [2012] reported that the observed waves have different wavelengths in WB1, WB2, and WB3. In order to cover these observed range of wavelengths, they considered two different runs for the 1-D Vlasov code, i.e, Run 1 and Run 2. They had taken the initial conditions for the simulation close to the observations, so as to make relevant comparisons between simulations and observations. Further, they compared the results of both the runs with the observations at WB1, WB2, and WB3. They were able to explain the properties of the high-frequency electrostatic waves observed at WB2 and WB3. But they did not provide a clear explanation for the observed low-frequency wave at WB1. For our model we have considered the exact parameters of the initial electron distribution of both the runs as given by *Tao et al.* [2012]. Since *Tao et al.* [2012] have normalized the velocity by the thermal velocity of the κ electron, $V_{t1} = \sqrt{T_e/m_e}$, and time by inverse of electron plasma frequency, $\omega_{\mathrm{pe}} = \sqrt{4\pi N_0 e^2/m_e}$, therefore, we convert the parameters to our normalizations. We have studied individually the results of both the runs. The numerical results of both the runs are compared with the observations at WB1 and WB2/WB3. Henceforth, the parameters and results corresponding to two runs will be designated as Run 1 and Run 2 as in *Tao et al.* [2012]. The normalized parameters considered for the numerical computations are Run 1—$\kappa = 6$, $n_{b0} = 0.01$, $\sigma_b = 0.0025$, and $V_{b0} = 17.14$ and Run 2—$\kappa = 6$, $n_{b0} = 0.015$, $\sigma_b = 0.01$, and $V_{b0} = 17.14$. *Tao et al.* [2012] do not give the number densities of heavier ions and the temperature of protons and heavier ions. Therefore, we have taken their values corresponding to the solar wind plasma, as described [*Mangeney et al.*, 1999; *Lakhina and Singh*, 2015]. The slow solar wind parameters are as follows: $n_{i0} = 0.05$, $\sigma_p = 0.2$, and $\sigma_i = 0.4$. This is valid as the lunar wake is refilled by the solar wind plasma through ambipolar diffusion. The normalized parameters considered in this paper for both Run 1 and Run 2 are listed in Table 2.

Table 2. The Normalized Parameters Corresponding to Run 1 and Run 2 [*Tao et al.*, 2012]

	Run 1	Run 2
κ	6	6
n_{p0}	0.9	0.9
n_{i0}	0.05	0.05
n_{e0}	0.99	0.985
n_{b0}	0.01	0.015
σ_p	0.2	0.2
σ_i	0.4	0.4
σ_b	0.0025	0.01
V_{b0}	17.14	17.14

For parameters corresponding to both the runs, we observe all three modes, i.e., slow and fast ion-acoustic mode and electron-acoustic mode.

For the normalized parameters relevant to the lunar wake plasma of Run 1, $n_{i0}=0.05$, $n_{b0}=0.01$, $\sigma_p=0.2$, $\sigma_i=0.4$, $\sigma_b = 0.0025$, and $\kappa = 6$, we observed that the slow ion-acoustic mode supports only positive potential soliton. The polarity of the soliton is consistent with the sign of the third derivative evaluated at $M = M_0$, as given by equation (9). Figure 2a shows the variation of Sagdeev potential $S(\phi, M)$ versus the normalized electrostatic potential ϕ for various values of the Mach number for the slow ion-acoustic soliton. The amplitude is found to increase with the increase in the Mach number, till the upper limit $M_{\max}$ is reached. $M_{\max}$ is the maximum Mach number beyond which the soliton solution ceases to exist. Here the upper limit $M_{\max}$ on the Mach number is provided by the restriction that the heavier ion density, n_i, be real. This is consistent with the observations of *Rubia et al.* [2016]. Figure 2b shows the profiles of normalized potential ϕ with ξ. The solitons exhibit a symmetric potential profiles. Here we observe that the soliton amplitude increases with increase in the Mach number, whereas the width decreases. The corresponding electric field profiles which exhibit bipolar nature are shown in Figure 2c. The electric field amplitude increases with the increase in the Mach number. Figure 2d shows the fast Fourier transform (FFT) power spectra of the electric field corresponding to Mach number $M = 0.5610$ for WB1. The frequency peak in the spectra occurs at 32.51 Hz, which corresponds to $0.01f_{pe}$ ($f_{pe} = 3237.78$ Hz) that agrees with the observed frequency peak near WB1 in Figure 1. It is found that the frequency, f, in the range of ∼(6.5–266.67) Hz, corresponding to ∼(0.002–0.08) f_{pe}, contributes maximum to the electric field structure for WB1. Figure 2e shows the FFT power spectra for the same Mach number for WB2/WB3. The maximum frequency contribution is in the range ∼(12.76–650.13) Hz, corresponding to ∼(0.002–0.1) f_{pe} ($f_{pe} = 6349.82$ Hz). The frequency peak occurs at 63.68 Hz, corresponding to $0.01f_{pe}$. For both cases, the upper limit on the frequency, f, is taken at the cutoff power of −80 dB. It is important to mention that throughout the paper, the cutoff power is taken at a value beyond which the power spectrum approaches to noise levels. Moreover, for both WB1 and WB2/WB3 the power in the power spectrum is found to decrease as frequency increases. Here we can see that the frequency range for both WB1 and WB2/WB3 is almost similar.

The fast ion-acoustic mode corresponding to Run 1 is found to support only positive potential soliton which is validated by the sign of equation (9). Figure 3a shows the variation of Sagdeev potential $S(\phi, M)$ versus the normalized electrostatic potential ϕ for various values of the Mach number for the fast ion-acoustic soliton. The pseudopotential profile shows a trend similar to that of the slow ion-acoustic soliton. Here the upper limit $M_{\max}$ on the Mach number is provided by the restriction that the lighter ion density, n_p, be real. This conforms with the limitation on the fast ion-acoustic soliton as reported by *Rubia et al.* [2016]. The normalized potential and the electric field also follow a trend similar to the slow ion-acoustic soliton as shown in Figures 3b and 3c, respectively. Figures 3d and 3e correspond to the FFT power spectra of the electric field corresponding to Mach number $M = 1.275$ for WB1 and WB2/WB3, respectively. The frequency, f, is in the range of ∼(14.79–1698.24) Hz, which corresponds to ∼(0.004–0.52) f_{pe}, and contributes maximum to the electric field structure for WB1. While for WB2/WB3, the maximum contribution is in the range ∼(28.97–5794.29) Hz, corresponding to ∼(0.004–0.91) f_{pe}. The cutoff power is considered as −40 dB. The frequency peak occurs at 29.58 Hz for WB1 and at 57.94 Hz for WB2/WB3. The frequency peak corresponds to ∼ $0.009f_{pe}$ for both WB1 and WB2/WB3. This frequency value is closer to the observed frequency of ∼ $0.01f_{pe}$ at WB1 [*Tao et al.*, 2012].

The electron-acoustic mode corresponding to Run 1 supports only negative potential solitons. The third derivative evaluated at $M = M_0$ has negative polarity. The Sagdeev potential, electrostatic potential, and the electric field profile follow a similar trend to that of slow ion-acoustic solitons as shown in Figure 4. The upper limit $M_{\max}$ on the Mach number is provided by the restriction that the beam electron density, n_b, be real. Figures 4d and 4e correspond to the FFT power spectra of the electric field corresponding to Mach number

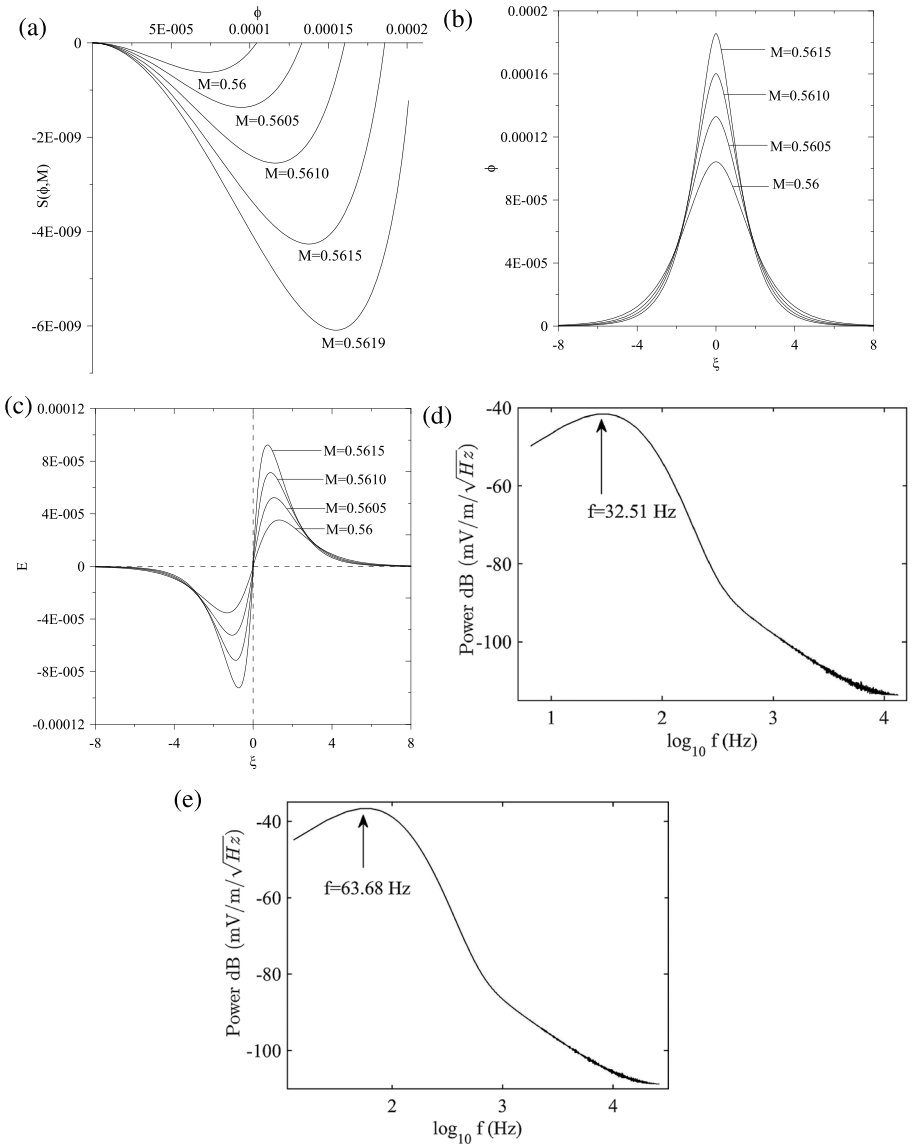

Figure 2. Run 1: (a) Variation of Sagdeev potential $S(\phi, M)$ versus the normalized electrostatic potential ϕ for the slow ion-acoustic mode for the normalized parameters corresponding to Run 1: $n_{i0} = 0.05$, $n_{p0} = 0.9$, $n_{b0} = 0.01$, $n_{e0} = 0.99$, $\sigma_p = 0.2$, $\sigma_i = 0.4$, $\sigma_b = 0.0025$, $v_{b0} = 17.14$ and $\kappa = 6$. (b) Variations of normalized potential ϕ versus ξ. (c) Variation of normalized electric field E versus ξ. (d) The fast Fourier transform (FFT) power spectra of the electric field corresponding to $M = 0.5610$ for WB1. The x axis represents the $\log_{10} f$, where f is the frequency in hertz. The y axis represents the power of the electric field expressed in units of decibel (mV/m/$\sqrt{Hz}$). (e) The FFT power spectra for WB2/WB3.

$M = 22.95$ for WB1 and WB2/WB3, respectively. The frequency, f, is in the range of ~(266.07–10641) Hz, corresponding to ~(0.08–3.29) f_{pe}, and contributes maximum to the electric field structure for WB1. While for WB2/WB3 the maximum contribution is in the range ~(521.19–35481.33) Hz corresponding to ~(0.08–5.59) f_{pe}. The frequency peak occurs at 797.99 Hz for WB1 and at 1563.15 Hz for WB2/WB3. Both the frequency peaks correspond to $0.25 f_{pe}$, which falls in the observed frequency range of (0.1–0.4) f_{pe} at both WB1 and WB2/WB3 [*Tao et al.*, 2012]. The power spectrum tends to noise level for frequencies beyond 50 kHz for both WB1 and WB2/WB3. Here the cutoff power is taken as −60 dB for both WB1 and WB2/WB3.

For the normalized parameters corresponding to Run 2, $n_{i0} = 0.05$, $n_{b0} = 0.015$, $\sigma_p = 0.2$, $\sigma_i = 0.4$, $\sigma_b = 0.01$, and $\kappa = 6$, we observed that the slow ion-acoustic solitons and electron-acoustic solitons show a trend and the frequency range similar to that of Run 1.

Here, for the first time, we report the coexistence of both positive and negative polarity solitons for the given parameters of Run 2 for fast ion-acoustic mode in the presence of κ electrons. The fast ion-acoustic mode is

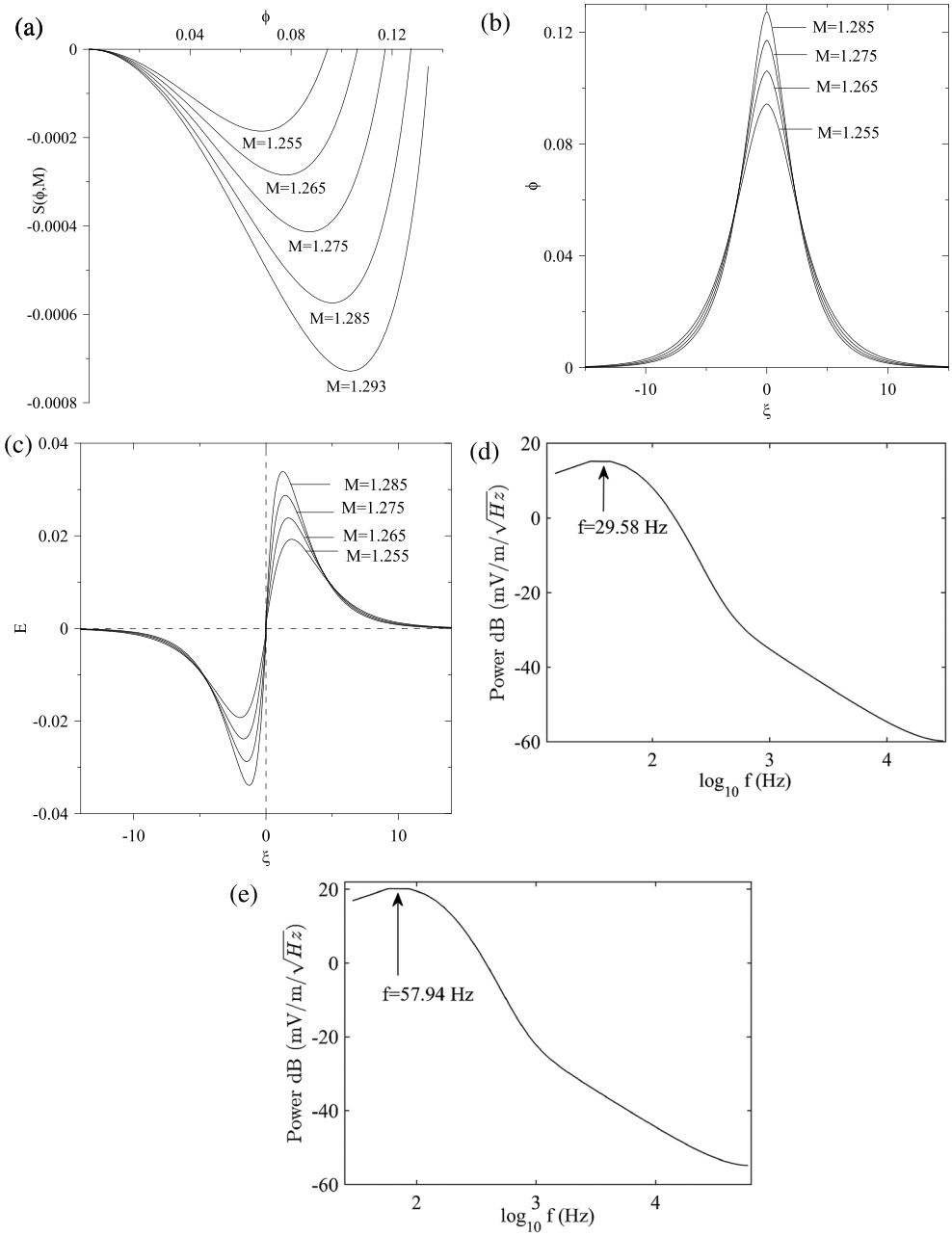

Figure 3. Run 1: (a) Variation of Sagdeev potential $S(\phi, M)$ versus the normalized electrostatic potential ϕ for the fast ion-acoustic mode for the normalized parameters corresponding to Run 1. (b) Variations of normalized potential ϕ versus ξ. (c) Variation of normalized electric field E versus ξ. (d and e) The FFT power spectra of the electric field corresponding to $M = 1.275$ for WB1 and WB2/WB3, respectively.

usually found to support positive potential solitons [*Lakhina et al.*, 2008b; *Lakhina and Singh*, 2015; *Rubia et al.*, 2016]. In this case, the sign of the third derivative (equation (9)) evaluated at $M = M_0$ is found to be positive. It is found that the positive as well as negative potential soliton has finite amplitude at $M = M_0$. Figure 5a shows the variation of Sagdeev potential $S(\phi, M)$ versus the normalized electrostatic potential ϕ for various values of the Mach number for the fast ion-acoustic solitons. The dotted lines correspond to the negative potential solitons, while the solid lines correspond to positive potential solitons. It is found that the range of Mach numbers over which the negative potential solitons exists is narrow as compared to the Mach number range over which positive potential soliton exists. For positive potential solitons, we have $M_0 = 1.217 \leq M < M_{max} = 1.3008$, while for negative potential solitons, we have $M_0 = 1.217 \leq M < M_{max} = 1.232$.Here the upper limit

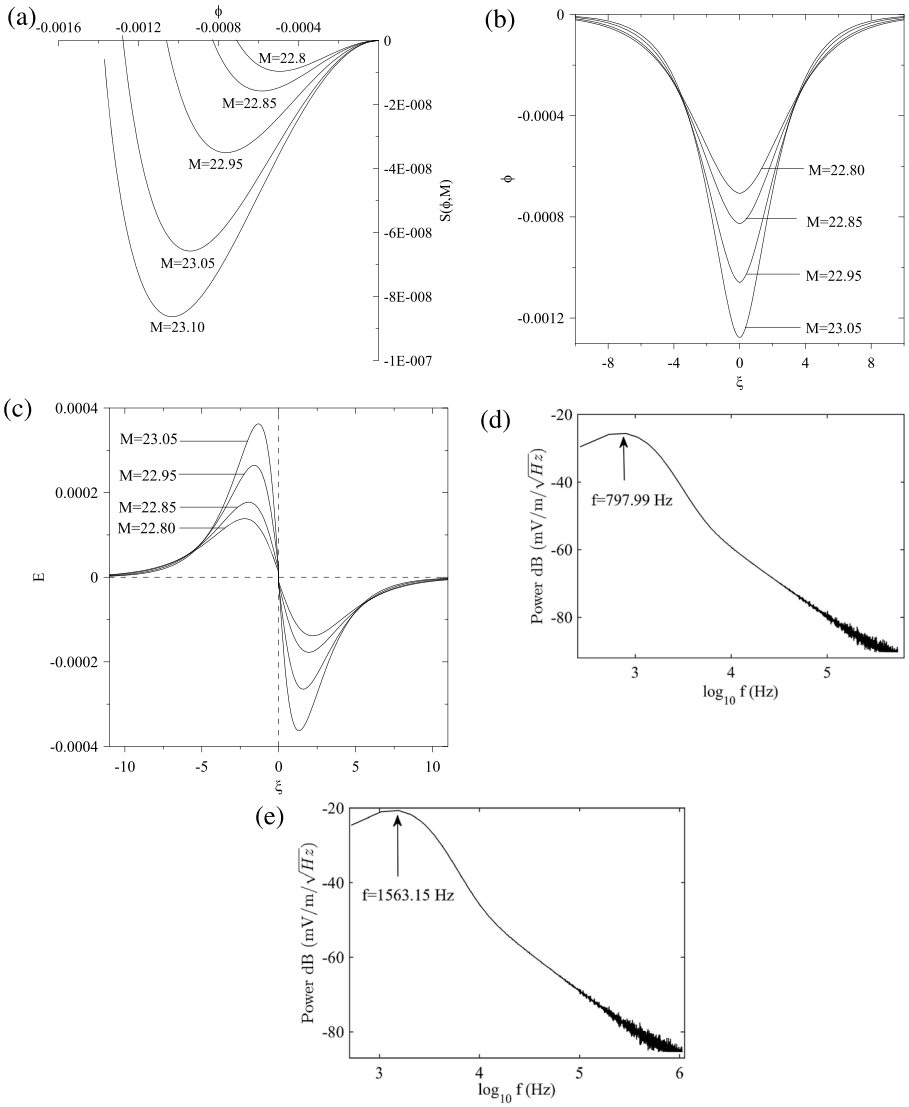

Figure 4. Run 1: (a) Variation of Sagdeev potential $S(\phi, M)$ versus the normalized electrostatic potential ϕ for the electron-acoustic mode for the normalized parameters corresponding to Run 1. (b) Variations of normalized potential ϕ versus ξ. (c) Variation of normalized electric field E versus ξ. (d and e) The FFT power spectra of the electric field corresponding to $M = 22.95$ for WB1 and WB2/WB3, respectively.

M_{max} on the Mach number in case of positive potential soliton is provided by the restriction that the lighter ion density, n_p, be real. However, in case of negative potential solitons the restriction on the maximum amplitude is provided by the requirement that the electron beam number density, n_b, be real. Further, for a given Mach number, the amplitude of negative potential soliton is lesser than the amplitude of positive potential soliton. However, in both the cases the amplitude increases with increase in the Mach number. The potential and the electric field also show a similar trend as depicted in Figures 5b and 5c, respectively.

Figures 5d and 5e depict the FFT power spectra of the electric field of positive potential soliton, corresponding to Mach number $M = 1.225$ for WB1 and WB2/WB3, respectively. The maximum contribution of the frequency to the electric field structure of positive potential soliton is in the range ~(3.55–1099) Hz, corresponding to ~(0.001–0.34) f_{pe} for WB1, and ~(6.95–3280.95) Hz, corresponding to ~(0.001–0.52) f_{pe} for WB2/WB3. Figures 5f and 5g correspond to the FFT power spectra of the negative potential soliton. The maximum contribution of the frequency to the electric field structure of negative potential soliton is in the range ~(3.55–1116.86) Hz, corresponding to ~(0.001–0.34) f_{pe} for WB1, and ~(6.96–3854.78) Hz, corresponding to ~(0.001–0.61) f_{pe} for WB2/WB3. Here the cutoff power is taken as −60 dB. For WB1, the peak frequency for the

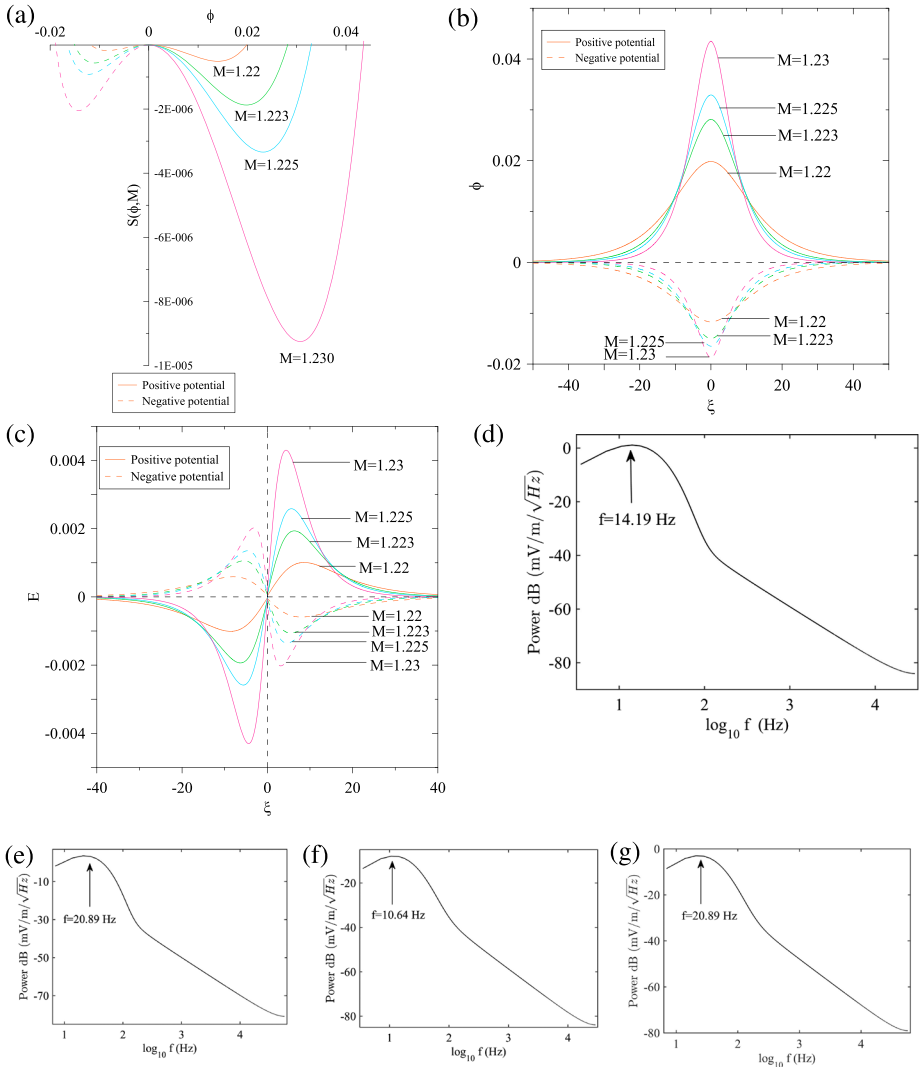

Figure 5. Run 2: (a) Variation of Sagdeev potential $S(\phi, M)$ versus the normalized electrostatic potential ϕ for the fast ion-acoustic mode for the normalized parameters corresponding to Run 2: $n_{i0} = 0.05$, $n_{p0} = 0.9$, $n_{b0} = 0.015$, $n_{e0} = 0.985$, $\sigma_p = 0.2$, $\sigma_i = 0.4$, $\sigma_b = 0.01$, $v_{b0} = 17.14$, and $\kappa = 6$. (b) Variations of normalized potential ϕ versus ξ. (c) Variation of normalized electric field E versus ξ. (d and e) The FFT power spectra of the electric field profile of the positive potential soliton corresponding to $M = 1.225$ for WB1 and WB2/WB3, respectively. (f and g) The FFT power spectra of the electric field profile of the negative potential soliton for WB1 and WB2/WB3, respectively.

positive potential solitons occurs at 14.19 Hz which corresponds to $0.004f_{pe}$, and for the negative potential soliton, the peak occurs at 10.64 Hz which corresponds to $0.003f_{pe}$. This matches with the observed frequency of $0.004f_{pe}$ near WB1. However, for WB2/WB3 the peak frequency occurs at 20.89 Hz corresponding to $0.003f_{pe}$ for both positive and negative potential solitons. This is lower than the reported frequency of $0.1f_{pe}$ near WB2/WB3.

The properties of the ESWs in terms of unnormalized quantities, such as their velocities, V, width, W, magnitude of the electric field, E, and peak frequency, f_{peak} corresponding to the maximum power in the spectrum for both Run 1 and Run 2 corresponding to WB1 and WB2/WB3 are listed in Tables 3 and 4, respectively. Here the width is defined as the full width at half maximum. The lower value of the frequency peak, f_{peak}, corresponds to the peak power in the spectrum of lower velocity soliton.

For numerical estimation of the physical properties of the electrostatic waves (given in Tables 3 and 4), we have used the parameters of *Tao et al.* [2012]: temperature of electron, $T_e = 28$ eV and total number density of electrons, $n_0 = 0.13$ cm^{-3} for WB1, while for WB2/WB3, we have used the parameters $T_e = 22.64$ eV and

Table 3. Properties of Electrostatic Solitary Waves for Run 1 Corresponding to WB1 and WB2/WB3[a]

			WB1				WB2/WB3			
	Mode	Polarity	V (km s^{-1})	E (mV m^{-1})	W (m)	f_{peak} (f_{pe})	V (km s^{-1})	E (mV m^{-1})	W (m)	f_{peak} (f_{pe})
Run 1	Slow ion-acoustic	+ve	28.91–29.08	0.0003–0.026	1330.76–261.79	0.002–0.01	26–26.15	0.0005–0.046	610.16–120.03	0.002–0.01
	Fast ion-acoustic	+ve	61.86–113.89	0.0082–9.52	7439.19–479.95	0.001–0.01	55.64–60.11	0.0145–16.79	3410.92–220.06	0.0008–0.01
	Electron-acoustic	−ve	1169.48–1195.37	0.0043–0.104	1243.5–436.316	0.08–0.25	1051.79–1075.07	0.0076–0.1832	570.15–200.05	0.08–0.25

[a]Here corresponding to WB1, temperature of κ electron, $T_e = 28$ eV, and total equilibrium number density, $n_0 = 0.13$ cm^{-3}. For WB2/WB3, temperature of κ electron, $T_e = 22.64$ eV, and total equilibrium number density, $n_0 = 0.5$ cm^{-3}. Here V is soliton velocity, E is electric field, W is soliton width, and f_{peak} corresponds to peak power in the spectrum. f_{pe} is the electron plasma frequency, $f_{pe} = 3237.78$ Hz for WB1, and $f_{pe} = 6349.82$ Hz for WB2/WB3.

$n_0 = 0.5$ cm^{-3} as given in Table 1. For the parameters corresponding to WB1, the ion-acoustic speed, $C_a = 52$ km s^{-1}, the effective hot Debye length, $\lambda_{de} = 109$ m, and the effective proton plasma frequency, $f_{pp} = 474.69$ Hz. For WB2/WB3, we have $C_a = 46$ km s^{-1}, $\lambda_{de} = 50$ m, and $f_{pp} = 930.95$ Hz.

The following section collates the numerical results of both Run 1 and Run 2 with the observations at WB1 and WB2/WB3.

5. Comparison With the Observations

From Tables 3 and 4, we see that the velocity of the electron-acoustic solitons is of the order of ∼1100 km s^{-1} (WB1, Run 1), ∼1300 km s^{-1} (WB1, Run 2), ∼1000 km s^{-1} (WB2/WB3, Run 1), and ∼1200 km s^{-1} (WB2/WB3, Run 2), while that of the slow ion-acoustic solitons is around ∼28.95 km s^{-1} (WB1) and ∼26.05 km s^{-1} (WB2/WB3), and the fast ion-acoustic soliton is around ∼(62–113) km s^{-1} (WB1, Run 1), ∼63 km s^{-1} (WB1, Run 2), and ∼57 km s^{-1} (WB2/WB3). Since for the Run 1 and Run 2 all the three types of solitons can exist simultaneously, there will be a considerable velocity spread in soliton velocities ranging from ∼30 to 1300 km s^{-1}. This compares very well with the estimated phase velocities of the orders of ∼1000 km s^{-1} by *Tao et al.* [2012].

The maximum electric field amplitude for the slow ion-acoustic solitons is in the range of ∼(0.0003–0.026) mV m^{-1} (WB1) and ∼(0.0005–0.046) mV m^{-1} (WB2/WB3). For fast ion-acoustic soliton the range of the electric field amplitude is ∼(0.0082–9.52) mV m^{-1} (WB1, Run 1), ∼(0.0145–16.79) mV m^{-1} (WB2/WB3, Run 1), ∼(0.038–9.7) mV m^{-1} (WB1, Run 2, positive potential solitons), ∼(0.066–17.106) mV m^{-1} (WB2/WB3, Run 2, positive potential solitons), ∼(0.019–0.58) mV m^{-1} (WB1, Run 2, negative potential solitons), and ∼(0.033–1.028) mV m^{-1} (WB2/WB3, Run 2, negative potential solitons), and for electron-acoustic soliton the range is ∼(0.0043–0.104) mV m^{-1}. Since all the three modes exist simultaneously, taken together, their electric fields would have amplitudes in the range of ∼0.0003 to ∼17 mV m^{-1} which compares excellently with the observed electric field amplitudes of 5 to 15 mV m^{-1} [*Tao et al.*, 2012].

The width of the slow ion-acoustic soliton is in the range of ∼(261.79–1330.76) m (WB1, Run 1), ∼(120.03–610.16) m (WB2/WB3, Run 1), ∼(239.97–1221.68) m (WB1, Run 2), and ∼(110.03–560.15) m (WB2/WB3, Run 2) and that of the fast ion-acoustic soliton is in the range of ∼(479.95–7439.19) m (WB1, Run 1), ∼(220.06–3410.92) m (WB2/WB3, Run 1), ∼(479.95–6501.11) m (WB1, Run 2, positive potential soliton),

Table 4. Properties of Electrostatic Solitary Waves for Run 2 Corresponding to WB1 and WB2/WB3[a]

			WB1				WB2/WB3			
	Mode	Polarity	V (km s^{-1})	E (mV m^{-1})	W (m)	f_{peak} (f_{pe})	V (km s^{-1})	E (mV m^{-1})	W (m)	f_{peak} (f_{pe})
Run 2	Slow ion-acoustic	+ve	28.92–29.09	0.0004–0.027	1221.68–239.97	0.002–0.01	26.01–26.16	0.0008–0.047	560.15–110.03	0.002–0.01
	Fast ion-acoustic	+ve	63.00–67.34	0.038–9.7	6501.11–479.95	0.0008–0.01	56.66–60.56	0.066–17.106	2980.8–220.06	0.001–0.01
	Fast ion-acoustic	−ve	63.00–63.78	0.019–0.58	8028.21–1112.605	0.0008–0.006	56.66–57.36	0.033–1.028	3680.99–510.14	0.0005–0.005
	Electron-acoustic	−ve	1348.09–1368.79	0.004–0.07	1199.87–436.32	0.18–0.56	1212.42–1231.05	0.007–0.12	550.15–200.05	0.09–0.28

[a]Here corresponding to WB1, temperature of κ electron, $T_e = 28$ eV, and total equilibrium number density, $n_0 = 0.13$ cm^{-3}. For WB2/WB3, temperature of κ electron, $T_e = 22.64$ eV, and total equilibrium number density, $n_0 = 0.5$ cm^{-3}. Here $f_{pe} = 3237.78$ Hz for WB1 and $f_{pe} = 6349.82$ Hz for WB2/WB3 and f_{peak} corresponds to peak power in the spectrum.

∼(220.06–2980.8) m (WB2/WB3, Run 2, positive potential soliton), ∼(1112.605–8028.21) m (WB1, Run 2, negative potential soliton), and ∼(510.14–3680.99) m (WB2/WB3, Run 2, negative potential soliton). The width of the electron-acoustic solitons lies in the range ∼(436.32–1243.5) m (WB1, Run 1), ∼(200.05–570.15) m (WB2/WB3, Run 1), ∼(436.32–1199.87) m (WB1, Run 2), and ∼(200.05–550.15) m (WB2/WB3, Run 2). Here the higher value of width corresponds to the lower velocity values. As all three modes exist simultaneously, the range of the soliton widths varies as ∼(110.03–8028.21) m which is in good agreement with the estimated wavelengths range of a few hundred meters to a couple of thousand meters [*Tao et al.*, 2012].

From Tables 3 and 4, the peak frequency, f_{peak}, for slow ion-acoustic soliton varies as ∼(6.47–34.2) Hz (WB1) corresponding to ∼(0.002–0.01) f_{pe} and ∼(12.7–66.99) Hz (WB2/WB3) corresponding to ∼(0.002–0.01) f_{pe}. The peak frequency of fast ion-acoustic soliton is in the range ∼(3.46–41.11) Hz (WB1, Run 1) corresponding to ∼(0.001–0.01) f_{pe}, ∼(5.09–80.92) Hz (WB2/WB3, Run 1) corresponding to ∼(0.0008–0.01) f_{pe}, ∼(2.64–41.5) Hz (WB1, positive potential soliton, Run 2) corresponding to ∼(0.0008–0.01) f_{pe}, ∼(6.92–77.62) Hz (WB2/WB3, positive potential soliton, Run 2) corresponding to ∼(0.001–0.01) f_{pe}, ∼(2.64–17.86) Hz (WB1, negative potential soliton, Run 2) corresponding to ∼(0.0008–0.006) f_{pe}, and ∼(3.46–34.99) Hz (WB2/WB3, negative potential soliton, Run 2) corresponding to ∼(0.0005–0.005) f_{pe}. The peak frequency for electron-acoustic soliton varies as ∼(261.81–803.53) Hz (WB1, Run 1) corresponding to ∼(0.08–0.25) f_{pe}, ∼(512.86–1573.98) Hz (WB2, Run 1) corresponding to ∼(0.08–0.25) f_{pe}, and ∼(591.56–1803.02) Hz (WB1, WB2/WB3, Run 2) corresponding to ∼(0.18–0.56) f_{pe} for WB1 and ∼(0.09–0.28) f_{pe} for WB2/WB3. Since all the three modes exist simultaneously for both the runs, taken together, their peak frequencies vary as ∼(2.64–1803.02) Hz corresponding to ∼(0.0008–0.56) f_{pe} for WB1 and ∼(0.0005–0.28) f_{pe} for WB2/WB3 which matches with the reported electrostatic wave frequencies (0.01–0.4) f_{pe} [*Tao et al.*, 2012].

6. Conclusions

We have proposed an alternative model for the existence of electrostatic waves in the lunar wake in terms of slow and fast ion- and electron-acoustic solitons. The main results of the paper are summarized below:

1. Slow and fast ion-acoustic solitons and electron-acoustic solitons can exist in the lunar wake in the presence of protons, alpha particles, electron beam, and suprathermal electrons with κ distribution.
2. The slow ion-acoustic mode supports only positive potential solitons. The electron-acoustic mode supports only negative potential solitons, while for certain parameters, fast ion-acoustic mode supports the coexistence of both positive and negative potential solitons.
3. For the plasma parameters in the lunar wake corresponding to Run 1 and Run 2 of *Tao et al.* [2012], our model predicts the simultaneous existence of slow and fast ion-acoustic and electron-acoustic solitons. The FFT of these solitons produces power spectra which have peaks between ∼(3–1800) Hz. This corresponds to frequency ∼(0.001–0.56) f_{pe} which is in very good agreement with the observed low-frequency electrostatic waves with frequency ∼0.01 f_{pe} at WB1 and the high-frequency waves with frequency ∼(0.1–0.4) f_{pe} at WB1 and WB2/WB3 in the lunar wake [*Tao et al.*, 2012].
4. Taken together, the slow and fast ion-acoustic and electron-acoustic solitons have widths, electric fields, and velocities in the range of ∼(100–8000) m, ∼(0.0003–17) mV m^{-1}, and ∼(30–1300) km s^{-1}, respectively. These appear to be in good agreement with the wavelengths, amplitudes, and phase velocities of the observed electrostatic waves in the lunar wake.

Acknowledgments
G.S.L. thanks the National Academy of Sciences, India, for the support under the NASI-Senior Scientist Platinum Jubilee Fellowship scheme. For theoretical model, the data input in this manuscript is used from published work of *Tao et al.* [2012]. Authors would like to thank Bharati Kakad for her help in FFT.

References

Bale, S. D., P. J. Kellogg, D. E. Larson, R. P. Lin, K. Goetz, and R. P. Lepping (1998), Bipolar electrostatic structures in the shock transition region: Evidence of electron phase space holes, *Geophys. Res. Lett.*, *25*, 2929–2932.

Baluku, T. K., M. A. Hellberg, and F. Verheest (2010), New light on ion acoustic solitary waves in a plasma with two-temperature electrons, *Europhys. Lett.*, *91*, 15001, doi:10.1209/0295-5075/91/15001.

Bosqued, J. M. et al. (1996), Moon-solar wind interaction: First results from the WIND/3DP experiment, *Geophys. Res. Lett.*, *23*, 1259–1262.

Buti, B. (1980), Ion-acoustic holes in a two-electron-temperature plasma, *Phys. Lett. A*, *76*, 251–254.

Devanandhan, S., S. V. Singh, and G. S. Lakhina (2011), Electron acoustic solitary waves with kappa-distributed electrons, *Phys. Scr.*, *84*, 025507, doi:10.1088/0031-8949/84/02/025507.

Devanandhan, S., S. V. Singh, G. S. Lakhina, and R. Bharuthram (2012), Electron acoustic waves in a magnetized plasma with kappa distributed ions, *Phys. Plasmas*, *19*, 082314, doi:10.1063/1.4743015.

Ergun, R. E., C. W. Carlson, J. P. McFadden, F. S. Mozer, L. Muschietti, I. Roth, and R. J. Strangeway (1998), Debye-scale plasma structures associated with magnetic-field-aligned electric fields, *Phys. Rev. Lett.*, *81*, 826–829.

Hashimoto, K., et al. (2010), Electrostatic solitary waves associated with magnetic anomalies and wake boundary of the Moon observed by KAGUYA, *Geophys. Res. Lett.*, *37*, L19204, doi:10.1029/2010GL044529.

Kakad, A. P., S. V. Singh, R. V. Reddy, G. S. Lakhina, S. G. Tagare, and F. Verheest (2007), Generation mechanism for electron acoustic solitary waves, *Phys. Plasmas*, *14*, 052305, doi:10.1063/1.2732176.

Kakad, A., B. Kakad, C. Anekallu, G. Lakhina, Y. Omura, and A. Fazakerley (2016), Slow electrostatic solitary waves in Earth's plasma sheet boundary layer, *J. Geophys. Res. Space Physics*, *121*, 4452–4465, doi:10.1002/2016JA022365.

Kojima, H., H. Matsumoto, S. Chikuba, S. Horiyama, M. Ashour-Abdalla, and R. R. Anderson (1997), Geotail waveform observations of broadband/narrowband electrostatic noise in the distant tail, *J. Geophys. Res.*, *102*, 14,439–14,455.

Lakhina, G. S., and S. V. Singh (2015), Generation of weak double layers and low-frequency electrostatic waves in the solar wind, *Sol. Phys.*, *290*, 3033–3049, doi:10.1007/s11207-015-0773-1.

Lakhina, G. S., A. P. Kakad, S. V. Singh, and F. Verheest (2008a), Ion- and electron-acoustic solitons in two-electron temperature space plasmas, *Phys. Plasmas*, *15*, 062903, doi:10.1063/1.2930469.

Lakhina, G. S., S. V. Singh, A. P. Kakad, F. Verheest, and R. Bharuthram (2008b), Study of nonlinear ion- and electron-acoustic waves in multi-component space plasmas, *Nonlinear Processes Geophys.*, *15*, 903–913.

Lakhina, G. S., S. V. Singh, A. P. Kakad, M. L. Goldstein, A. F. Viñas, and J. S. Pickett (2009), A mechanism for electrostatic solitary structures in the Earth's magnetosheath, *J. Geophys. Res.*, *114*, A09212, doi:10.1029/2009JA014306.

Lakhina, G. S., S. V. Singh, A. P. Kakad, and J. S. Pickett (2011), Generation of electrostatic solitary waves in the plasma sheet boundary layer, *J. Geophys. Res.*, *116*, A10218, doi:10.1029/2011JA016700.

Lakhina, G. S., S. V. Singh, and A. P. Kakad (2014), Ion acoustic solitons/double layers in two-ion plasma revisited, *Phys. Plasmas*, *21*, 062311, doi:10.1063/1.4884791.

Maharaj, S. K., R. Bharuthram, S. V. Singh, and G. S. Lakhina (2012a), Existence domains of arbitrary amplitude nonlinear structures in two-electron temperature space plasmas: I. Low-frequency ion-acoustic solitons, *Phys. Plasmas*, *19*, 072320, doi:10.1063/1.4737895.

Maharaj, S. K., R. Bharuthram, S. V. Singh, and G. S. Lakhina (2012b), Existence domains of arbitrary amplitude nonlinear structures in two-electron temperature space plasmas: II. High-frequency electron-acoustic solitons, *Phys. Plasmas*, *19*, 122301, doi:10.1063/1.4769174.

Mangeney, A., C. Salem, C. Lacombe, J. L. Bougeret, C. Perche, R. Manning, P. J. Kellogg, K. Goetz, S. J. Monson, and J. M. Bosqued (1999), WIND observations of coherent electrostatic waves in the solar wind, *Ann. Geophys.*, *17*, 307–320.

Matsumoto, H., H. Kojima, T. Miyatake, Y. Omura, M. Okada, I. Nagano, and M. Tsutsui (1994), Electrostatic solitary waves (ESW) in the magnetotail: BEN wave forms observed by GEOTAIL, *Geophys. Res. Lett.*, *21*, 2915–2918.

Matsumoto, H., X. H. Deng, H. Kojima, and R. R. Anderson (2003), Observation of electrostatic solitary waves associated with reconnection on the dayside magnetopause boundary, *Geophys. Res. Lett.*, *30*(6), 1326, doi:10.1029/2002GL016319.

Miyake, T., Y. Omura, and H. Matsumoto (2000), Electrostatic particle simulations of solitary waves in the auroral region, *J. Geophys. Res.*, *105*(A10), 23,239–23,249.

Ness, N. F., K. W. Behannon, C. S. Scearce, and S. C. Cantarano (1967), Early results from the magnetic field experiment on Lunar Explorer 35, *J. Geophys. Res.*, *72*, 5769–5778.

Ogilvie, K. W., J. T. Steinberg, R. J. Fitzenreiter, C. J. Owen, A. J. Lazarus, W. M. Farrell, and R. B. Torbert (1996), Observations of the lunar plasma wake from the WIND spacecraft on December 27, 1994, *Geophys. Res. Lett.*, *23*, 1255–1258.

Olivier, C. P., S. K. Maharaj, and R. Bharuthram (2015), Ion-acoustic solitons, double layers and supersolitons in a plasma with two ion- and two electron species, *Phys. Plasmas*, *22*, 082312, doi:10.1063/1.4928884.

Pickett, J. S, J. R. Franz, J. D. Scudder, J. D. Menietti, D. A. Gurnett, G. B. Hospodarsky, R. M. Braunger, P. M. Kintner, and W. S. Kurth (2001), Plasma waves observed in the cusp turbulent boundary layer: An analysis of high time resolution wave and particle measurements from the Polar spacecraft, *J. Geophys. Res.*, *106*, 19,081–19,099.

Pickett, J. S., J. D. Menietti, D. A. Gurnett, B. Tsurutani, P. M. Kintner, E. Klatt, and A. Balogh (2003), Solitary potential structures observed in the magnetosheath by the Cluster spacecraft, *Nonlinear Processes Geophys.*, *10*, 3–11.

Rubia, R., S. V. Singh, and G. S. Lakhina (2016), Existence domains of electrostatic solitary structures in the solar wind plasma, *Phys. Plasmas*, *23*, 062902, doi:10.1063/1.4953892.

Rufai, O. R., R. Bharuthram, S. V. Singh, and G. S. Lakhina (2012), Low frequency solitons and double layers in a magnetized plasma with two temperature electrons, *Phys. Plasmas*, *19*, 122308.

Sagdeev, R. Z. (1966), Cooperative phenomena and shock waves in collisionless plasmas, in *Leontovich, M. A.*, vol. 4, Rev. Plasma Phys., p. 23, Consultants Bureau, New York.

Singh, S. V., S. Devanandhan, G. S. Lakhina, and R. Bharuthram (2013), Effect of ion temperature on ion-acoustic solitary waves in a magnetized plasma in presence of superthermal electrons, *Phys. Plasmas*, *20*, 012306.

Summers, D., and R. M. Thorne (1991), The modified plasma dispersion function, *Phys. of Fluids B: Plasma Phys.*, *3*, 1835–1847, doi:10.1063/1.859653.

Tao, J. B., et al. (2012), Kinetic instabilities in the lunar wake: ARTEMIS observations, *J. Geophys. Res.*, *117*, A03106, doi:10.1029/2011JA017364.

Umeda, T., Y. Omura, and H. Matsumoto (2004), Two-dimensional particle simulation of electromagnetic field signature associated with electrostatic solitary waves, *J. Geophys. Res.*, *109*, A02207, doi:10.1029/2003JA010000.

Washimi, H., and T. Taniuti (1966), Propagation of ion-acoustic solitary waves of small amplitude, *Phys/ Rev. Lett.*, *17*, 996–998.

Wiehle, S., et al. (2011), First lunar wake passage of ARTEMIS: Discrimination of wake effects and solar wind fluctuations by 3D hybrid simulations, *Planet. Space Sci.*, *59*, 661–671.